RSC Advances

PAPER

View Article Online
View Journal | View Issue

Cite this: *RSC Adv.*, 2017, **7**, 13536

Fractal analysis of pre-reduced Pt/TiO_2 catalysts for formaldehyde oxidation†

Jiaxi Peng,[a] Xiaoxin Wu*[a] and Shudong Wang*[b]

Received 21st February 2017
Accepted 23rd February 2017

DOI: 10.1039/c7ra02161e

rsc.li/rsc-advances

The amount of reactive sites, usually dispersed noble atoms, on the top of a catalyst rough surface is characterized within the framework of fractal geometry. The surface fractal dimension d_{fs} was calculated from their nitrogen adsorption isotherms using an A. V. Neimark model. It was found that the catalysts pre-reduced at different temperatures showed different d_{fs} values and distinct formaldehyde oxidation performance. As expected, a good agreement between performance and d_{fs} values was achieved. These results are significant for our understanding of the nature of the catalyst's surface roughness and illustrate the importance of considering difference in surface fractal geometry in analyzing catalytic behavior.

1. Introduction

Some hydrocarbons with a Reid vapor pressure of over 10.3 kPa at normal pressure and temperature are defined as volatile organic compounds (VOCs) and recognized as primary contributors to air pollution, because of their toxic or malodorous nature, or indirectly as ozone precursors and smog precursors. Formaldehyde (HCHO) is considered as the major indoor pollutant emitted from the widely used building and decorative materials in airtight buildings, which is one of the dominating VOCs. Exposure to indoor air containing a low concentration of HCHO for a long time may have adverse effects on human health.[1] Thus, great efforts have been made to reduce the indoor emission of HCHO to satisfy the stringent environmental regulations.[2–5] More recently, catalytic oxidation of HCHO was achieved over a Pt/TiO_2 catalyst even at room temperature.[6] Furthermore, we found that the Pt/TiO_2 catalyst pre-reduced at different temperatures affected its efficiency significantly,[7,8] considered it may be deal with the catalyst surface fractal geometry.

Many studies based on theoretical[9–11] and computer simulations[11–13] have shown that the surface roughness degree of materials distinctly affects the mass transfer in the pores, especially by surface diffusion[9,10] and Knudsen diffusion.[11,12] Some simulation results have shown that the selectivity, especially in the competing diffusion-limited reactions[13,14] could be affected by the degree of heterogeneous catalyst surface geometry. So, it is significant to quantify the degree of surface structural heterogeneity. The concept of fractal may offer a tool by which the rough surface may be both characterized and mathematically simulated. Characterization of catalysts in terms of fractal geometry has been found useful during the last decades.[15–21] Many experimental studies[22–27] of heterogeneous catalytic processes adapted fractal analysis to show that the fractal nature of the active phase may be responsible for the variation in reactivity. The basic characteristic of fractal systems is their fractal dimension which can be determined with the help of various methods such as adsorption,[28,29] small angle scattering (SAXS and SANS),[30,31] porometry,[32] electron microcopy,[33,34] atomic force microscopy,[35] *etc.*

A. V. Neimark *et al.*[36] proposed a simple model based on the nitrogen adsorption isotherm in the region of polymolecular adsorption and corresponds respectively to the scale range from molecular sizes to 300 Å to discriminate the surface geometry. Employment of this method enables to obtain information on a lower limit of possible fractality scales. Such a model is also a complement to testify for or against the fractal properties of adsorbents on larger scales up to 1000 Å. The conclusions based on nitrogen adsorption isotherms are significant for a critical analysis of the results obtained from other non-adsorption methods such as small angle scattering techniques.[37]

Our previous studies[7,8] showed that the Pt/TiO_2 catalytic performance is related with many factors, such as the Pt chemical state, TiO_2 surface structure, *etc.* as well mentioned in many studies.[38,39] Although the active sites of the catalysts in the reaction are reduced platinum nanoparticles, the mass transfer of reactants in the surface pores is very critical due to the fact that catalytic oxidation of formaldehyde is a diffusion limited intrinsic reaction. In this study, we try to analyze the catalysts surface geometry with A. V. Neimark model[36] using N_2 adsorption isotherms replacement of atomic force microscopy and other methods, help to understand the role of fractal geometry in mass transfer in catalyst pores, especially in the diffusion-limited catalytic reactions.

[a]*Department of Polymer Materials and Chemical Engineering, East China Jiaotong University, Nanchang 330013, P. R. China. E-mail: wuxiaoxin@ecjtu.edu.cn*

[b]*Dalian Institute of Chemical Physics, Dalian National Laboratory for Clean Energy, Chinese Academy of Sciences, Dalian 116023, P. R. China. E-mail: wangsd.@dicp.ac.cn*

† Electronic supplementary information (ESI) available. See DOI: 10.1039/c7ra02161e

2. Experiments

2.1. Materials preparation

Aqueous ammonia (Shenyang, 12.5%) was drop wisely added to the vigorously stirred solution of titanium sulfate at ambient temperature until its pH reached 7.5. After aging for 16 h, the white hydrous titania was then filtered and washed several times by deionized water until there was no SO_4^{2-} in the filtration ($Ba(NO_3)_2$ test), and then the precipitate was calcined at 600 °C (ramp rate is 10 °C min^{-1}) for 2 h to obtain TiO_2 powder. Supported platinum catalysts (0.6 wt%) were prepared by the method of incipient wetness impregnation of as-prepared TiO_2 powder, using H_2PtCl_6 as the precursor. Impregnated samples were dried at 120 °C overnight, then heated to 500 °C in 30 minutes, and calcined for 3 h in air. The catalysts were pre-reduced with 150 ml min^{-1} hydrogen at 300, 450 and 700 °C, which were denoted as PT300, PT450 and PT700, respectively.

2.2. N_2 adsorption

N_2 adsorption isotherms of the samples were obtained at −196 °C on an ASAP 2010 Micromeritics instrument. The specific surface area was determined by using the linear portion of the Brunauer–Emmett–Teller (BET) model, and the average pore size was calculated by using the Barrett–Joyner–Halenda (BJH) formula from the desorption branch of the N_2 adsorption isotherm. Prior to theses measurements, the samples were degassed in vacuum at 300 °C for 2 h.

2.3. Catalyst performance test

The pre-reduced catalyst performance for the oxidation of formaldehyde was tested as described in our previous study.[7]

3. Model

As well known, low temperature (at 77 K) adsorption isotherms of nitrogen on numerous adsorbents of different origin obey a single empirical law in the region of polymolecular adsorption up to the beginning of capillary condensation. When it takes place, the isotherm measured on a porous solid is proportional to the so called "standard" isotherm or *t*-curve of de Boer, which corresponds to a nonporous smooth surface.

$$N(P/P_0) = N_{mi} + S_{me}N_{st}(P/P_0) \quad (1)$$

where $N(P/P_0)$ (mmol g^{-1}) is the adsorption on a given sample, $N_{st}(P/P_0)$ (mmol m^{-2}) is the adsorption on a smooth surface of unit area at the same relative pressure (P/P_0), an excess N_{mi} (mmol g^{-1}) is the adsorption in micropores, and a factor of proportionality, S_{me} (m^2 g^{-1}), is the specific surface area of the mesopores. Several comparative methods for calculating the specific surface area are based on this property of nitrogen isotherms. As considering porous materials without any appreciable amount of micropores, the value of S_{me} does not differ significantly from the BET surface area. At the same time, the value of N_{mi} is negligible relative to the total adsorption as $P/P_0 \rightarrow 1$ and may be either positive or negative depending on the peculiarities of submonolayer adsorption.

A low sensitivity of the standard isotherm $N_{st}(P/P_0)$ to the origin of solid surface is the advantage of nitrogen as a probe gas. The universality of $N_{st}(P/P_0)$ implies that the adsorbate–adsorbent interactions as well as the chemical and geometrical surface heterogeneity on molecular level affect the nitrogen adsorption only in the early stages and are reduced during the monolayer filling. A possible explanation is that the quadrupole–quadrupole interactions between adsorbed molecules of nitrogen predominate over the adsorbate–adsorbent interactions. This is one reason why the influence of the surface chemical origin on nitrogen adsorption is not as intrinsic as for other adsorbates and why nitrogen is an ideal adsorbate for an analysis of the geometrical structure of porous solids.

A. V. Neimark[36] proposed to use nitrogen adsorption isotherms for the discrimination of surface irregularities, particularly fractal type irregularities. The idea is as follows. The existence of surface irregularities of a size more than the molecular diameter of nitrogen (~4 Å) should lead to a deviation from the linear relationship (eqn (1)) in the region of polymolecular adsorption. On the other hand, if the adsorption isotherm on an explored surface obeys eqn (1) over a certain range of relative pressures, then it can be concluded that in the corresponding range of scales the given surface is similar to a smooth surface and therefore not fractal. In the region where the experimental nitrogen isotherm does not fit the empirical law (eqn (1)), it is possible to investigate fractal properties using corresponding models. When this occurs, the upper limit of validity of eqn (1) is the lower limit of possible fractality.

To provide a quantitative comparison among surfaces, it is convenient to employ a certain algebraic equation for the standard isotherm. Because of its empirical nature, there is no reliable theoretical equation. The Frenkel–Halsey–Hill (FHH) equation for a standard nitrogen isotherm,

$$N_{st}(P/P_0) = K/(\ln(P_0/P))^{1/m} \quad (2)$$

describes numerous experimental data quite well. Only in exceptional cases, *e.g.*, for adsorption on Au (111),[40] does the exponent m equal 3, corresponding to the theoretical value for adsorption ruled by adsorbate–adsorbent dispersion interactions. For the most part, the empirical FHH equation with $2 < m < 3$ is used to fit experimental data. Dubinin *et al.*[41] recommend eqn (2) with parameters $m = 2.24$, $K = 0.0157$ mmol m^{-2} as a standard nitrogen isotherm on various inorganic and carbon nonporous solids in the range of relative pressures from ~0.1 to ~0.9. Their investigations also confirm satisfactory agreement between the FHH equation with these parameters and nitrogen isotherms on a number of mesoporous solids in the region of polymolecular adsorption. The standard isotherm in this form is employed here.

The deviations from eqn (1) are caused by the capillary condensation in mesopores of size more than ~10 Å. The fractal properties on the scales more than 10–200 Å can be investigated on the basis of nitrogen adsorption isotherms by means of a thermodynamic method. The thermodynamic method employs

the following equation valid for capillary condensation on a fractal dimension d_{fs}:

$$\log[S_{lg}(P/P_0)] = \text{const} - (d_{fs} - 2)\log[\alpha_c(P/P_0)] \quad (3)$$

here, $S_{lg}(P/P_0)$ is the area of condensed nitrogen-vapor equilibrium interface at a given value of relative pressure calculated by integrating the isotherm from the current value. $N(P/P_0)$, to the maximal value, N_{max}, available as $P/P_0 \rightarrow 1$ according to the Kiselev equation,

$$S(P/P_0) = (RT/\sigma)\int_{N(P/P_0)}^{N_{max}} \ln(P_0/P)\mathrm{d}N \quad (4)$$

where σ is the surface tension of liquid nitrogen, R is the universal gas constant, and T is the temperature, $\alpha_c(P/P_0)$ is the mean radius of curvature of this interface calculated by the Kelvin equation,

$$\alpha_c(P/P_0) = 2\sigma\upsilon_m/RT\ln(P_0/P) \quad (5)$$

where υ_m is the molar volume of liquid nitrogen. In fact, eqn (3) represents the common relationship for the area of a fractal surface; $S_{lg}(P/P_0)$ is interpreted as the area of solid surface measured by a yardstick of size equal to $\alpha_c(P/P_0)$.

The combination of the comparative method, based on eqn (1), and the thermodynamic method, based on eqn (3), makes it possible to discriminate the fractal properties of mesoporous materials in the range of scales from ~4 Å (molecular diameter of nitrogen) to ~1000 Å on the basis of one experimental nitrogen adsorption isotherm.

An analysis of low temperature nitrogen adsorption isotherms provides the capability to determine the surface fractality. The comparative method, based on eqn (1) and (2), gives a definite negative answer or a "soft" positive answer as to whether or not the surface of a given mesoporous material may be considered as a fractal. In the scale range corresponding to the linear relationship between the nitrogen isotherm on a given sample and the standard isotherm on a smooth surface, the fractal properties do not exist definitely. The upper limit of similarity of these isotherms is the lower limit of the region of possible fractality. On the other hand, in the region of nonlinearity of the comparative plot, only additional study can confirm the existence of fractal properties. In this case the thermodynamic method, based on eqn (3)–(5), is useful. This conclusion is also supported by their investigations of such materials as silica gels, porous glasses, natural apatite and coal.[32]

4. Results and discussion

The XRD patterns of the catalysts pre-reduced at different temperatures ranged from 300 °C to 700 °C are shown in Fig. 1. From the patterns, there are no diffraction peaks characteristic of platinum indicating that platinum is well dispersed on TiO_2. When pre-reduced below 700 °C, the catalysts show three distinctive peaks at 25.3°, 37.6° and 48.0° as the same to pure TiO_2, which corresponding to the anatase (101), (004) and (200) crystal planes (JCPDS 21-1272), indicating that pure anatase phase existed in the catalysts. The physical properties of the Pt/TiO_2 catalysts pre-reduced at different temperatures were respectively summarized in Table 1. As we can see from the results in Table 1, all the catalysts have nearly negligible micropore surface area, the mesopore surface area value of S_{me} does not differ significantly from the BET surface area S_{BET}, which could fit the above model well.

The PT300 catalyst pre-reduced at 300 °C is a mesoporous catalyst, the pore size distribution is relatively narrow with a nominal pore diameter of 120 Å, specific surface area S_{BET} = 64.83 $m^2\ g^{-1}$, and pore volume V_0 = 0.240 $cm^3\ g^{-1}$. The low temperature nitrogen adsorption isotherm on the sample of PT300 employed is shown in Fig. 2a.

The adsorption and desorption branches form well defined hysteresis loop of type H1 by the IUPAC classification. Such an adsorption–desorption loop with clear boundaries is characteristic of mesoporous solids and indicates a relatively narrow

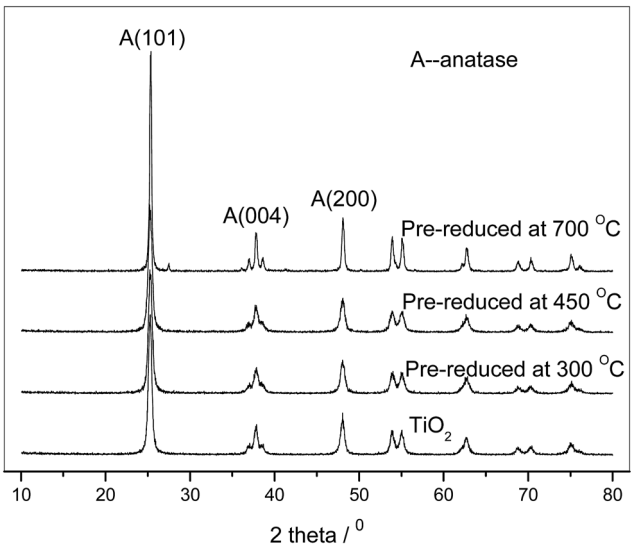

Fig. 1 XRD patterns measured for Pt/TiO_2 pre-reduced at different temperatures.

Table 1 The surface parameters of the catalysts pre-reduced at different temperatures

		PT300	PT450	PT700
Surface area $m^2\ g^{-1}$	Micropores S_{mi}	2.67	1.87	0.92
	Mesopores S_{me}	62.16	59.66	19.57
	BET surface area	64.83	61.53	20.49
Pore volume $cm^3\ g^{-1}$		0.240	0.235	0.165
Pore diameter nm		12.49	11.68	28.36
BET fitted range p/p_0		0.06–0.20	0.06–0.20	0.07–0.20
Correlation coefficient		0.9999	0.9999	0.9999
BET constant C		102.19	101.83	99.65

mesoporous size distribution in the sample. The reversible part of the isotherm below the hysteresis corresponds to the mono- and polymolecular adsorption on the surface of mesoporous and to reversible capillary condensation in the surface indentations.

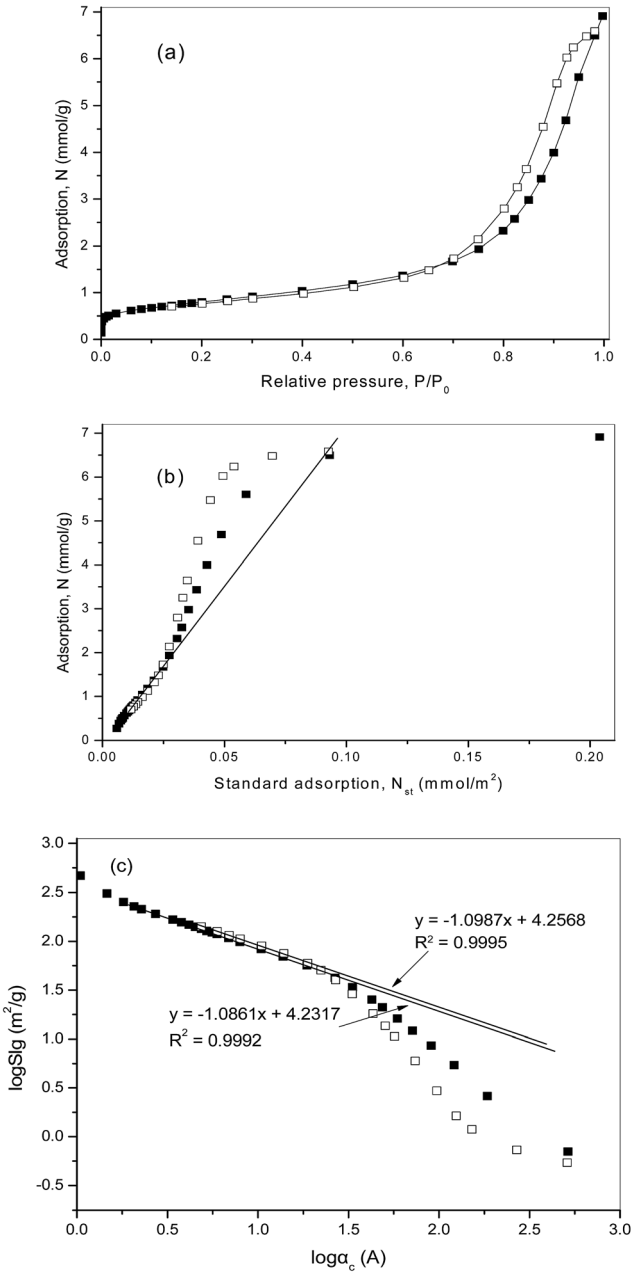

Fig. 2 Fractal analysis of a catalyst pre-reduced at 300 °C. (a) Low temperature nitrogen adsorption isotherm, $N(P/P_0)$; (■) adsorption, (□) desorption. (b) Comparative plot. $N(P/P_0)$, experimental adsorption isotherm [(■) adsorption, (□) desorption]; $N_{st}(P/P_0)$, standard adsorption isotherm. The straight line corresponds to the linear regression of the initial part of the plot in the range of relative pressures 0.01–0.60 with the slope $S_{me} = 62.16$ m^2 g^{-1}. (c) Results of calculations, by means of the thermodynamic model, of the surface area, S_{lg}, of condensed nitrogen as a function of the current mean radius of curvature, α_c; (■) calculated from adsorption data, (□) calculated from desorption data. The straight lines correspond to the linear regression for the adsorption plot with the surface fractal dimension $d_{fs} = 2.629 \pm 0.003$ and for the desorption plot with the surface fractal dimension $d_{fs} = 2.662 \pm 0.003$.

In Fig. 2b, the adsorption isotherm $N(P/P_0)$ is replotted by employing standard coordinates of the comparative method as a function of the standard nitrogen adsorption isotherm $N_{st}(P/P_0)$ (mmol m^{-2}). The isotherm is a linear function of the standard isotherm $N_{st}(P/P_0)$ up to the relative pressure $P/P_0 = 0.60$, which is the upper limit of similarity of the adsorption process on the explored sample and on the smooth surface. The slope of the linear part of the plot is related to the value of mesopore surface area $S_{me} = 62.16$ m^2 g^{-1}, which is in close agreement with the BET specific surface area.

The departures of the comparative plot from linearity are observed long before the beginning of capillary hysteresis, which occurs at $P/P_0 = 0.70$. Such behavior suggests the existence of surface roughness on the scales more than 30 Å, which is quite less than the nominal pore diameter equal to 120 Å. In this region the process of capillary condensation in the surface indentations and pores predominates and to assess the surface fractal properties of the sample we have used the A. V. Neimark model. In Fig. 2c, the two plots, based on the adsorption and desorption branches of the isotherm, respectively, are drawn employing standard coordinates of the model, $\log S_{lg}$ *versus* $\log \alpha_c$. The region of fractality corresponds to the linear part of the $\log S_{lg} - \log \alpha_c$ plot, the plot based on the adsorption branch, testifies the fractal properties over a large scale range, where it can be regarded as linear. The result of linear regression in the range is presented by a straight line. The slope corresponds to the surface fractal dimension $d_{fs} = 2.629 \pm 0.003$. The plot, based on the desorption branch, is linear in a slightly broader scale range, that can be related to the influence of the irreversible desorption from mesopores in the hysteresis region. Linear regression of the desorption plot corresponds the surface fractal dimension $d_{fs} = 2.662 \pm 0.003$. The results obtained from adsorption and desorption branch data are very similarly close.

We emphasize that the lower limit of fractality, $\alpha_{min} = 5$ Å is related to the value of relative pressure $P/P_0 = 0.16$, which is a little less than the upper limit linearity of the comparative plot. The upper limit of fractality, $\alpha_{max} = 200$ Å, is comparable with the mean radius of mesopores. This is characteristic for a porous structure, where the pore network is constituted by channels with a relatively narrow size distribution and, at the same time, with rough walls. In the case, it is obvious that the mean radius of pore channels is the upper limit of possible fractality.

For the considered another sample of PT450, Pt/TiO_2 pre-reduced at 450 °C, the specific surface area $S_{BET} = 61.53$ m^2 g^{-1} and the pore volume $V_0 = 0.235$ cm^3 g^{-1} with a nominal pore diameter of 120 Å. The low temperature nitrogen adsorption isotherm, N, is presented in Fig. 3a as a function of the relative pressure, P/P_0, and in Fig. 3b as a function of standard isotherm, $N_{st}(P/P_0)$. The results of fractal analysis by means of the thermodynamic model are presented in Fig. 3c.

These results are quite similar to those for the sample of PT300 (Fig. 2). The comparative plot, Fig. 3b, is linear in the range of relative pressures, P/P_0, from 0.05 to 0.80 with a slope

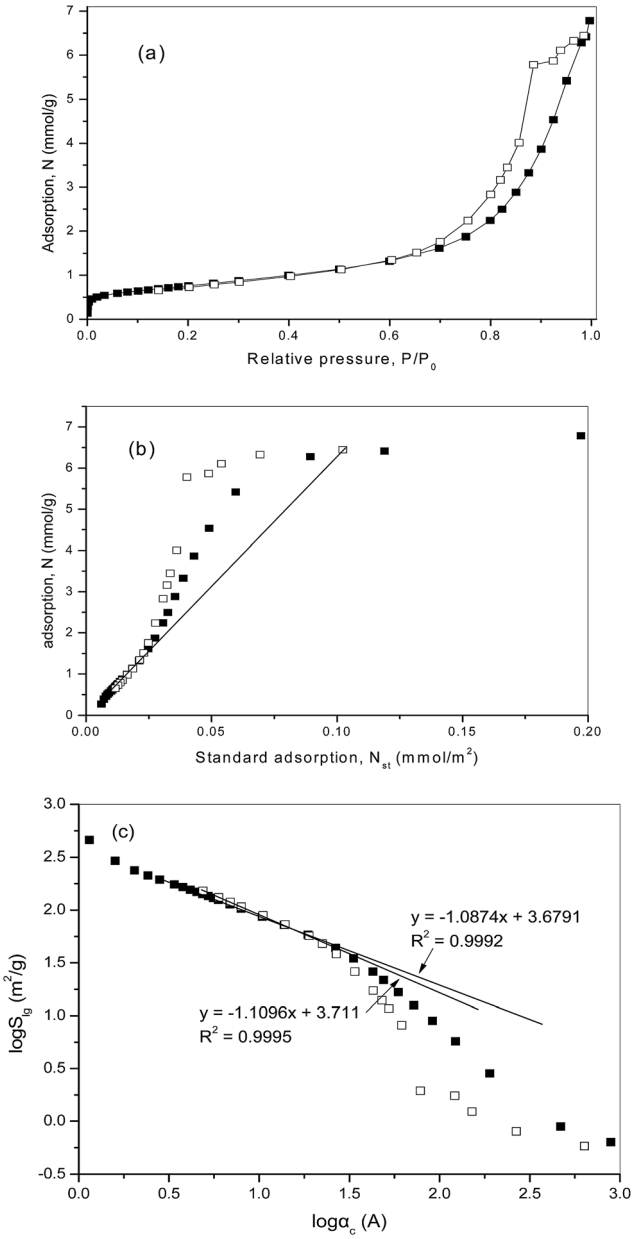

Fig. 3 Fractal analysis of a catalyst pre-reduced at 450 °C. (a) Low temperature nitrogen adsorption isotherm, $N(P/P_0)$; (■) adsorption, (□) desorption. (b) Comparative plot. $N(P/P_0)$, experimental adsorption isotherm [(■) adsorption, (□) desorption]; $N_{st}(P/P_0)$, standard adsorption isotherm. The straight line corresponds to the linear regression of the initial part of the plot in the range of relative pressures 0.05–0.80 with the slope $S_{me} = 59.66\ m^2\ g^{-1}$. (c) Results of calculations, by means of the thermodynamic method, of the surface area, S_{lg}, of condensed nitrogen as a function of the current mean radius of curvature, α_c; (■) calculated from adsorption data, (□) calculated from desorption data. The straight lines correspond to the linear regression for the adsorption plot with the surface fractal dimension $d_{fs} = 2.640 \pm 0.002$ and for the desorption plot with the surface fractal dimension $d_{fs} = 2.720 \pm 0.002$.

related to the value of mesopore surface area $S_{me} = 59.66\ m^2\ g^{-1}$ in close agreement with the BET surface area. The low limit of surface roughness is about 5 Å.

The log S_{lg} − log α_c plot (Fig. 3c) corresponds the fractal properties over the same scale range with the surface fractal dimension $d_{fs} = 2.640 \pm 0.002$ based on the adsorption branch, and the plot,

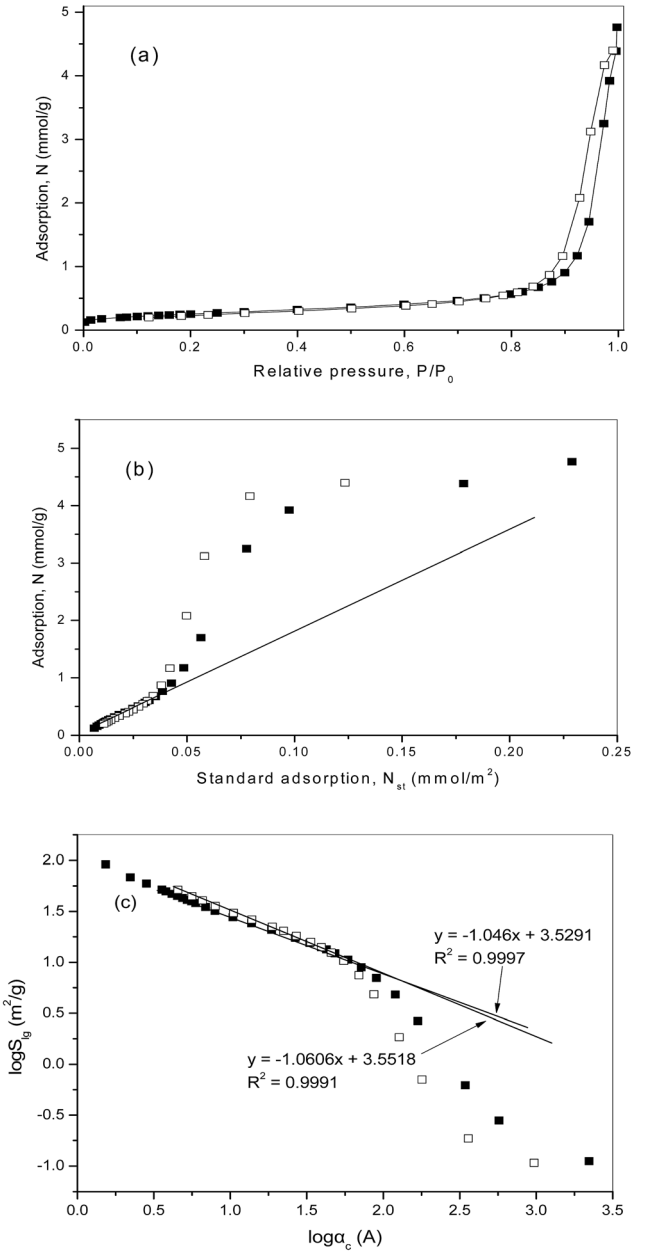

Fig. 4 Fractal analysis of a catalyst pre-reduced at 700 °C. (a) Low temperature nitrogen adsorption isotherm, $N(P/P_0)$; (■) adsorption, (□) desorption. (b) Comparative plot. $N(P/P_0)$, experimental adsorption isotherm [(■) adsorption, (□) desorption]; $N_{st}(P/P_0)$, standard adsorption isotherm. The straight line corresponds to the linear regression of the initial part of the plot in the range of relative pressures 0.01–0.50 with the slope $S_{me} = 19.57\ m^2\ g^{-1}$. (c) Results of calculations, by means of the thermodynamic method, of the surface area, S_{lg}, of condensed nitrogen as a function of the current mean radius of curvature, α_c; (■) calculated from adsorption data, (□) calculated from desorption data. The straight lines correspond to the linear regression for the adsorption plot with the surface fractal dimension $d_{fs} = 2.579 \pm 0.005$ and for the desorption plot with the surface fractal dimension $d_{fs} = 2.577 \pm 0.005$.

Table 2 The efficiency for catalytic oxidation of formaldehyde and the fractal dimension of the catalysts pre-reduced at different temperatures

Samples		PT300	PT450	PT700
Fractal dimension d_{fs}	Adsorption branch	2.629 ± 0.003	2.640 ± 0.002	2.579 ± 0.005
	Desorption branch	2.662 ± 0.003	2.720 ± 0.002	2.577 ± 0.005
Oxidation conditions: GHSV 30 000 cm^3 g^{-1} h^{-1}, HCHO 100 mg m^{-3}				
Formaldehyde conversion (%)	23 °C	39.4	42.1	13.2
	40 °C	76.5	78.4	19.2
	60 °C	88.9	94.9	41.7
	90 °C	95.7	99.0	89.3
	120 °C	97.8	99.8	96.8

based on the desorption branch, is linear over the same scale range, and the corresponding value of $d_{fs} = 2.720 \pm 0.002$.

For the considered third sample of PT700, Pt/TiO_2 pre-reduced at 700 °C, the specific surface area $S_{BET} = 20.49$ m^2 g^{-1} and the pore volume $V_0 = 0.165$ cm^3 g^{-1} with a nominal pore diameter of 280 Å. The low temperature nitrogen adsorption isotherm, N, is presented in Fig. 4a as a function of the relative pressure, P/P_0, and in Fig. 4b as a function of standard isotherm, $N_{st}(P/P_0)$. The results of fractal analysis by means of the thermodynamic model are presented in Fig. 4c.

These results are quite similar to those for the samples of PT300 and PT450 (Fig. 2 and 3). The comparative plot, Fig. 4b, is linear in the range of relative pressures, P/P_0, from 0.01 to 0.50 with a slope related to the value of mesopore surface area $S_{me} = 19.57$ m^2 g^{-1} in close agreement with the BET surface area. The low limit of surface roughness is about 5 Å.

The $\log S_{lg} - \log \alpha_c$ plot (Fig. 4c) corresponds the fractal properties over the same scale range with the surface fractal dimension $d_{fs} = 2.579 \pm 0.005$ based on the adsorption branch, and the plot, based on the desorption branch, is linear over the same scale range, corresponding the value of $d_{fs} = 2.577 \pm 0.005$.

The Pt/TiO_2 catalysts pre-reduced at different temperatures resulted in different catalysts surfaces geometry. The surface is the more complex; the more irregular, fine structure and rumple of the surface exist, which reflects in the fractal dimension being bigger. The fractal surfaces are more efficient than planar ones for diffusion limited reaction processes and therefore, fractal catalyst has an advantage compared to a non fractal one. The fractal dimension, d_{fs}, of the catalysts pre-reduced at different temperatures and the corresponding catalyst efficiency for the catalytic oxidation of formaldehyde are summarized in Table 2. Among all the catalysts, PT450 has the biggest fractal dimension value and in result it shows the highest activity at different temperatures.

5. Conclusions

A fractal analysis of low temperature nitrogen adsorption isotherms provides the capability to determine the surface geometry. The comparative method, based on eqn (1) and (2), gives a definite negative answer or "soft" positive answer as to whether or not the surface of a given mesoporous catalysts may be considered as a fractal. The thermodynamic model based on eqn (3)–(5) is useful to calculate the fractal properties. Among our presented catalysts, the catalyst pre-reduced at 450 °C has the biggest fractal dimension d_{fs}, and the efficiency for the catalysts used in catalytic oxidation of formaldehyde support the opinion that the bigger of the fractal dimension d_{fs}, the more efficient of the catalyst. The fractal analysis of the catalysts surface geometry could play an important role in the diffusion limited reactions.

Acknowledgements

The authors would like to express their gratitude for the financial support for the project by Jiangxi Province Education Department (GJJ150514) and China Sponsorship Council.

References

1 Y. Sekine, *Atmos. Environ.*, 2002, **36**, 5543–5547.
2 F. Wang, Q. Zhang, M. Sakurai and H. Kameyama, *Catal. Commun.*, 2007, **8**, 2171–2175.
3 L. Wang, R. Yunus, J. G. Li, P. L. Li, P. Y. Zhang and J. Kim, *Appl. Surf. Sci.*, 2015, **357**, 787–794.
4 S. Colussi, M. Boaro, L. Rogatis, A. Pappacena, C. Leitenburg, J. Llorca and A. Trovarelli, *Catal. Today*, 2015, **253**, 163–171.
5 F. Qi, B. Cheng, J. G. Yu and W. K. Ho, *J. Hazard. Mater.*, 2016, **301**, 522–530.
6 B. Zhang, H. He and K. Tanaka, *Catal. Commun.*, 2005, **6**, 211–214.
7 X. Peng and S. D. Wang, *Appl. Catal., B*, 2007, **73**, 282–291.
8 X. Peng and S. D. Wang, *J. Phys. Chem. C*, 2007, **111**, 9897–9904.
9 P. Rigby, *Langmuir*, 2002, **18**, 1613–1618.
10 P. Rigby, *Langmuir*, 2003, **19**, 364–376.
11 K. Malek and M. O. Coppens, *J. Chem. Phys.*, 2003, **119**, 2801–2811.
12 S. Wang, Z. F. Ma, H. Q. Yao and F. S. Liu, *Chem. Eng. Sci.*, 2013, **101**, 813–827.
13 A. Kriston, T. Y. Xie and B. N. Popov, *Electrochim. Acta*, 2014, **121**, 116–127.
14 P. Rigby and L. F. Gladden, *J. Catal.*, 1998, **180**, 44–50.
15 M. Wang and S. F. Li, *Ind. Eng. Chem. Res.*, 1997, **36**, 1598–1602.
16 K. Lee, *Ind. Eng. Chem. Res.*, 1998, **37**, 3939–3942.
17 A. Smith, A. Zoelle, Y. Yang, R. M. Rioux, N. G. Hamilton, K. Amakawa, P. K. Nielsen and A. Trunschke, *J. Catal.*, 2014, **312**, 170–178.

18 Z. Jelčič, Z. M. Samardžić and S. Zrnčević, *Appl. Catal., A*, 2013, **456**, 30–43.
19 M. He, N. T. Tung, Y. Adachi and K. Kobayashi, *Catal. Today*, 2016, **271**, 91–101.
20 I. Trypolskyi, T. M. Gurnyk and P. E. Strizhak, *Catal. Commun.*, 2011, **12**, 766–771.
21 R. Larraz, *Chem. Eng. J.*, 2002, **86**, 309–317.
22 O. Coppens and G. F. Froment, *Chem. Eng. Sci.*, 1996, **51**, 2283–2292.
23 F. Galindo-Hernández, J. M. Domínguez and B. Portales, *J. Power Sources*, 2015, **287**, 13–24.
24 A. Montesinos-Castellanos, E. Lima, J. A. de los Reyes and H. V. Lara, *J. Phys. Chem. C*, 2007, **111**, 13898–13904.
25 H. Abu Bakar, M. M. Bettahar, M. Abu Bakar, S. Monteverdi, J. Ismail and M. Alnot, *J. Catal.*, 2009, **265**, 63–71.
26 B. Jefferson, P. Jarvis, G. K. Bhagianathan, H. Smith, O. Autin, E. H. Goslan, J. MacAdam and I. Carra, *Chem. Eng. J.*, 2016, **288**, 359–367.
27 B. Guan, H. Lin, L. Zhu, B. Tian and Z. Huang, *Chem. Eng. J.*, 2012, **181–182**, 307–322.
28 Y. Zhang, H. Y. Cui, Z. Z. He, L. Su and D. G. Fu, *RSC Adv.*, 2016, **6**, 8639–8643.
29 F. Galindo-Hernández, J. A. Wang, L. F. Chen and X. Bokhimi, *J. Mater. Res.*, 2013, **28**, 3297–3309.
30 K. Sinko, V. Torma and A. Kovacs, *J. Non-Cryst. Solids*, 2008, **354**, 5466–5474.
31 X. Guo, K. Gao, A. Gutsche, M. Seipenbusch and H. Nirschl, *Powder Technol.*, 2015, **272**, 23–33.
32 M. Cuerda-Correa, A. Macias-Garcia, M. A. Diaz-Diaz and A. L. Ortiz, *Microporous Mesoporous Mater.*, 2008, **111**, 523–529.
33 S. Talu, S. Solaymani, M. Bramowicz, N. Naseri, S. Kulesza and A. Ghaderi, *RSC Adv.*, 2016, **6**, 27228–27234.
34 N. Sahoo and B. Kandasubramanian, *RSC Adv.*, 2014, **4**, 11331–11342.
35 S. Tălu, M. Bramowicz, S. Kulesza, A. Shafiekhani, A. Ghaderi, F. Mashayekhi and S. Solaymani, *Ind. Eng. Chem. Res.*, 2015, **54**, 8212–8218.
36 V. Neimark and K. K. Unger, *J. Colloid Interface Sci.*, 1993, **158**, 412–419.
37 A. Hohr, H. B. Neumann, P. W. Schmidt, P. Pfeifer and D. Avnir, *Phys. Rev. B: Condens. Matter Mater. Phys.*, 1988, **38**, 1462–1467.
38 A. Somorjai and J. Y. Park, *Angew. Chem., Int. Ed.*, 2008, **47**, 9212–9228.
39 Y. Oh, K. Qadir and J. Y. Park, *Catal. Lett.*, 2017, **147**, 39–45.
40 J. Krim and E. T. Watts, *A.I.Ch.E.*, New York, 1991.
41 M. Dubinin, L. I. Kataeva and V. I. Ulin, *Bull. Acad. Sci. USSR, Div. Chem. Sci.*, 1977, **26**, 459–463.